Food & Function

ROYAL SOCIETY OF CHEMISTRY

PAPER

View Article Online
View Journal | View Issue

Cite this: *Food Funct.*, 2023, **14**, 946

Glycyrrhizic acid alters the hyperoxidative stress-induced differentiation commitment of MSCs by activating the Wnt/β-catenin pathway to prevent SONFH†

Huihui Xu,[a,b] Liang Fang,[a,b] Qinghe Zeng,[a,b] Jiali Chen,[a,b] Houfu Ling,[a,b] Hanting Xia,[a,b] Qinwen Ge,[a,b] Congzi Wu,[a,b] Kaiao Zou,[a,b] Xu Wang,[a,b] Pinger Wang,[a,b] Wenhua Yuan,[a,b] Rui Dong,[a,b,c] Songfeng Hu,[d] Luwei Xiao,[a,b] Bangjian He,*[c] Peijian Tong*[a,b,c] and Hongting Jin*[a,b,c]

This study aimed to examine the *in vivo* and *in vitro* therapeutic effects of glycyrrhizic acid (GA) on steroid-induced osteonecrosis of the femoral head (SONFH), which is caused by the overuse of glucocorticoids (GCs). Clinically, we identified elevated oxidative stress (OS) levels and an imbalance in osteolipogenic homeostasis in SONFH patients compared to femoral neck fracture (FNF) patients. *In vivo*, we established experimental SONFH in rats *via* lipopolysaccharides (LPSs) combined with methylprednisolone (MPS). We showed that GA and Wnt agonist-S8320 alleviated SONFH, as evidenced by the reduced microstructural and histopathological alterations in the subchondral bone of the femoral head and the decreased levels of OS in rat models. *In vitro*, GA reduced dexamethasone (Dex)-induced excessive NOX4 and OS levels by activating the Wnt/β-catenin pathway, thereby promoting the osteogenic differentiation of mesenchymal stem cells (MSCs) and inhibiting lipogenic differentiation. In addition, GA regulated the expression levels of the key transcription factors downstream of this pathway, Runx2 and PPARγ, thus maintaining osteolipogenic homeostasis. In summary, we demonstrated for the first time that GA modulates the osteolipogenic differentiation commitment of MSCs induced by excessive OS through activating the Wnt/β-catenin pathway, thereby ameliorating SONFH.

Received 12th August 2022,
Accepted 1st December 2022

DOI: 10.1039/d2fo02337g

rsc.li/food-function

1. Introduction

Osteonecrosis of the femoral head (ONFH) is a progressive and destructive orthopaedic disease that predominantly progresses to the collapse of the femoral head.[1] In the USA, approximately 20 000–30 000 new cases of ONFH are diagnosed annually. Other reports estimate the annual incidence of ONFH to be between 75 000 and 150 000 in China and between 12 000 and 24 000 in Japan,[2,3] with steroid-induced osteonecrosis of the femoral head (SONFH) being the most prevalent type following prolonged or overdose of glucocorticoid (GC) therapy.[4] The World Health Organization (WHO) recommends the application of systemic GCs (*i.e.*, dexamethasone, Dex) for the adjuvant treatment of coronavirus disease 2019 (COVID-19).[5] Therefore, it is foreseeable that with the widespread prevalence of COVID-19 and the application of GCs, the number of patients diagnosed with SONFH will also be markedly enhanced in the near future. The difficulties in diagnosing and treating SONFH are predominantly due to the nebulous potential mechanisms. Accordingly, it is urgent and vital to comprehend the exact pathological mechanisms and develop novel and effective treatments to disrupt the process of SONFH.

Mesenchymal stem cells (MSCs), initially identified in adult bone marrow, can self-renew and differentiate into several cell lineages, including osteoblasts, chondrocytes, and adipocytes.[6] Pharmacological concentrations of GCs can suppress the bone formation and shift the lineage commitment of MSCs from the osteoblast lineage to the adipocyte lineage.[7,8] Although the exact mechanism of SONFH remains elusive, recent studies have demonstrated that bone marrow mesenchymal stem cells (BMSCs) isolated from SONFH patients have a reduced ability

[a]*The First College of Clinical Medicine, Zhejiang Chinese Medical University, Hangzhou, Zhejiang, 310053, China*
[b]*Institute of Orthopaedics and Traumatology of Zhejiang Province, Hangzhou, Zhejiang, 310053, China*
[c]*Department of Orthopaedic Surgery, The First Affiliated Hospital of Zhejiang Chinese Medical University, Hangzhou, Zhejiang, 310006, China*
[d]*Department of Orthopaedics and Traumatology, Shaoxing Hospital of Traditional Chinese Medicine, Shaoxing, Zhejiang, 312000, China*
† Electronic supplementary information (ESI) available. See DOI: https://doi.org/10.1039/d2fo02337g

to differentiate into bone tissue and tend to differentiate into adipose tissue due to prolonged exposure to GCs.[9,10] In addition, studies have shown that there is an oxidative stress (OS) microenvironment in the necrotic area of SONFH and that after femoral head necrosis, many inflammatory cells infiltrate and produce excessive reactive oxygen species (ROS), thus exacerbating the SONFH process.[6,11] Meanwhile, recent studies have indicated that excessive OS induces an imbalance in the osteolipogenic differentiation of MSCs.[12,13] So is osteolipogenic destabilization of MSCs caused by excessive OS a pivotal etiology and pathogenesis of SONFH? And how to effectively reduce OS levels and restore osteolipogenic homeostasis in MSCs?

Plant-based therapies derived from traditional Chinese medicine (TCM) have been used for refractory orthopedic diseases with widespread attention due to their safety effects.[14,15] Preceding studies have demonstrated that several herbs and their monomers could ameliorate SONFH in animal models and clinical trials.[16] With the rapid development of bioinformatics, network pharmacology has been extensively applied to identify the preventive and therapeutic targets of TCM.[17,18] Hopkins first proposed the concept of network pharmacology to elucidate the synergistic interactions and the underlying mechanisms of multi-compound and multi-target drugs by analyzing complex network interactions,[19] providing a new and effective method to reveal the mechanism of action of TCM monomers. Glycyrrhizic acid (GA) is one of the primary triterpenoid glycosides isolated from the roots and rhizomes of licorice.[20,21] It has been shown to enhance the effectiveness of other ingredients, reduce the toxicity of other drug-like agents, and improve the flavor of herbal formulas.[22] In addition, GA is known to exert various pharmacological effects, including antioxidative, antitumor, anti-inflammatory and antiviral.[21,23] Recently, it has been shown that GA promotes bone fracture healing by stimulating the osteogenic differentiation of BMSCs.[24] Meanwhile, GA has also been demonstrated to suppress adipogenesis by decreasing the expression of lipogenic transcription factors, thus maintaining lipid homeostasis.[25,26] Interestingly, these therapeutic mechanisms were intimately linked to the etiology and pathogenesis of SONFH. However, there are gaps regarding whether GA can treat SONFH and the potential mechanisms. Therefore, this study aimed to clarify the pathogenesis of SONFH and examine the therapeutic effect of GA on SONFH. Moreover, the possible therapeutic mechanisms involved were also explored.

2. Materials and methods

Patients

Our study was performed according to the Declaration of Helsinki. All methods were approved by the Research Ethics Committee of the First Affiliated Hospital of Zhejiang Chinese Medical University (Hangzhou, China; approval no. 2018-KL-005-02). Written informed consent was obtained from each donor with the permission of the Institutional Review Committee of the First Affiliated Hospital of Zhejiang Chinese Medical University. Patients diagnosed with terminal SONFH (stage III and IV according to the ARCO Classification System)[2,27] or femoral neck fracture (FNF) and decided to undergo a total hip arthroplasty at the First Affiliated Hospital of Zhejiang Chinese Medical University (Zhejiang, China) were recruited from October 2018 to February 2021. This study collected 30 SONFH and 20 FNF femoral head samples after femoral osteotomy and promptly stored them in liquid nitrogen pending use. Meanwhile, some of the specimens were taken for radiographic and histopathological examinations.

Prediction of GA and ONFH targets

The two-dimensional chemical structure of GA was acquired from PubChem (ESI Fig. 1A†). The "SMILES" format of GA was obtained by searching for "glycyrrhizic acid" and entered into the SwissTargetPrediction database. In addition, a comprehensive collection of the targets of GA was made through pharmMapper, the HERB database and the TargetNET database, and 713 genes associated with GA were integrated (ESI Table S1†). Then, 713 GA target genes were imported into the STRING database and 527 targets were identified by setting the highest confidence level (0.9) and hiding the nodes disconnected from the network (ESI Table S2†). Subsequently, each predictive target was imported to the UniProt database for selection. A total of 2314 ONFH-related targets were obtained by entering "osteonecrosis of the femoral head", "ONFH" and "femoral head necrosis" as keywords in the GeneCards database, followed by conversion of target IDs using the UniProt database.

Construction of PPI network

GA targets were screened using the STRING database, including direct and indirect interactions among proteins, and confidence scores were calculated. We set scores above 0.9 as high confidence and removed free nodes to construct a protein–protein interaction (PPI) network for GA. The PPI network is composed of proteins that interact with each other to participate in various aspects of life processes, such as biological signaling, regulation of gene expression, and energy and material metabolism.

Construction of GA-ONFH core target network

The GA-ONFH composite targets were acquired by matching the GA targets with the ONFH targets. A VENN map was drawn using the OmicShare online mapping tool. In addition, the GA-ONFH core target network was constructed and visualized by Cytoscape, resulting in 268 intersecting targets (ESI Fig. 1B and Table S3†). The STRING database was employed to collect functionally relevant PPI data from the 268 targets, identifying 186 relevant potential genes (ESI Table S4†). Then, a network of pharmacological targets and functionally relevant PPIs for GA against ONFH was constructed (ESI Fig. 1C†).

Topology analysis

Nodes with topological importance in the interaction network were filtered out using the calculation of degree centrality,

betweenness centrality and proximity centrality, which measured the connections of a node with others and reflected the significance of a particular node.

GO function and KEGG pathway enrichment analysis

Gene Ontology (GO) and Kyoto Encyclopedia of Genes and Genomes (KEGG) functional enrichment analyses were conducted using the GA-ONFH core target network *via* the OmicShare online mapping tool, with the screening criteria adjusted to $p \leq 0.05$. The GO enrichment analyses focused on the biological processes (BPs), the cellular compositions (CCs) and the molecular functions (MFs) of the targets, while the KEGG enrichment analyses analyzed the underlying biological pathways and functions relevant to the targets.

Cell culture

C3H10T1/2 murine MSC line (ATCC Manassas, VA, USA) incubated in Dulbecco's modified Eagle's medium (DMEM) (HyClone, Logan, Utah, USA) with 10% fetal bovine serum (FBS) (Gibco, Grand Island, NY, USA) and 1% penicillin/streptomycin (Invitrogen, Carlsbad, California, USA) in a 5% CO_2 humidified incubator at 37 °C.

Cell proliferation detection

The doses of Dex (1 μM) (Selleck, Shanghai, China) and GA (5, 10, 20, 40, and 80 μM) (Selleck, Shanghai, China) were according to the previous studies.[28,29] Briefly, MSCs were seeded in 96-well plates with a density of 8×10^3 cells per well in 100 μL of medium with additional Dex or GA for 24 h, 48 h and 72 h. To detect MSC proliferation, 10 μL of CCK-8 solution (Beyotime, Shanghai, China) was added to each well and then cultured at 37 °C for another 2 h. Subsequently, the absorbance of each well was measured using a microplate reader at 450 nm.

Osteogenic differentiation and osteogenesis assay

Cells were subcultured into 24-well plates at 5×10^4 cells per well. After reaching 80% confluence, the cells were cultured in an osteoblast-induced medium (OIM, DMEM supplemented with 10% FBS, 50 μg ml^{-1} of ascorbic acid, and 10 mM β-glycerophosphate) to induce osteogenic differentiation and refreshed every 2 days. Simultaneously, 1 μM DEX and the respective medications were added to the OIM for 14 days in all groups except for the control group, where OIM was added only. ALP staining was performed by using a 1-Step™ NBT/BCIP Kit (Thermo Fisher Scientific, Waltham, Massachusetts, USA) following the manufacturer's procedure.

Adipogenic differentiation and adipogenesis assay

Cells were subcultured into 12-well plates at 1×10^5 cells per well. After reaching 80% confluence, the cells were cultured in an adipocyte-induced medium (AIM, DMEM supplemented with 10% FBS, 1 M dexamethasone, 0.5 mM methyl isobutyl xanthine, 10 g ml^{-1} of insulin, and 100 M indomethacin) to induce adipogenic differentiation for 2 days. Then, the cells were cultured in the following adipocyte-maintaining medium (AMM, DMEM supplemented with 10% FBS and 10 μg ml^{-1} of insulin) and refreshed every 2 days until 21 days. In addition, 1 μM DEX was added to the AMM along with the respective treatment until ORO staining in all groups except for the control group, where AMM was added only. Following the manufacturer's procedure, Oil red O staining was performed using an Oil red O Staining Kit (ScienCell, San Diego, California, USA).

Cell treatments

Cells were divided into the control group, the model group (treated with 1 μM Dex), the GA group (treated with 1 μM Dex and 80 μM GA), the Wnt/β-catenin pathway agonist-S8320 group (treated with 1 μM Dex and 10 μM S8320) (Selleck, Shanghai, China), and the GA plus Wnt/β-catenin pathway inhibitor-S8761 group (treated with 1 μM Dex and 80 μM GA and 100 nM S8761) (Selleck, Shanghai, China).

Intracellular ROS detection

The intracellular ROS level was detected using a fluorescent dye, 2′,7′-dichlorofluorescein diacetate (DCFH-DA; BB-470516; BestBio, Shanghai, China). Specifically, the cells were seeded in 12-well plates and treated with the respective drugs described above for 12 h. After rinsing three times, 10 μM DCFH-DA was added and incubated for 30 min at room temperature without light. Positive expression of ROS was observed by fluorescence microscopy (X-Cite® 120Q; Lumen Dynamics, Newtown, New Jersey, USA) and quantified by the Image-Pro software (Media Cybernetics, Silver Spring, Maryland, USA).

Reverse transcription-quantitative PCR (RT-qPCR)

MSCs were incubated in respective media for 3 days. Subsequently, total RNA was extracted using TRIzol® Reagent (Invitrogen, Carlsbad, California, USA), and cDNA was synthesized using a PrimeScript™ RT Reagent Kit (Takara, Beijing, China) according to the manufacturer's procedure. RT-qPCR was performed using SYBR® Premix Ex Taq™ II (Takara, Beijing, China). The primer sequences are presented in Table 1 and the relative mRNA expression was measured by the $2^{-\Delta\Delta Cq}$ method.

Western blotting

MSCs were incubated in respective media for 3 days and lysed on ice for 2 h in a radioimmunoprecipitation assay (RIPA) lysis buffer (CW Biotech, Beijing, China) containing ethylenediaminetetraacetic acid (EDTA)-free Protease Inhibitor Cocktail (Roche, Basle, Switzerland). The proteins were quantified using a Pierce™ BCA Protein Assay Kit (Thermo Fisher Scientific, Waltham, Massachusetts, USA), fractionated by sodium dodecyl sulfate-polyacrylamide gel electrophoresis, and then transferred to a nitrocellulose membrane. After blocking in the solution, which contains 5% of skim milk at room temperature for 1 h, the polyvinylidene fluoride membranes were incubated overnight at 4 °C with primary antibodies against β-catenin (diluted 1 : 5000, 51067-2-AP; Proteintech, Chicago, USA), nicotinamide adenine dinucleotide phosphate oxidase-4 (NOX4; diluted 1 : 1000, ET1607-4;

Table 1 Primer sequences for RT-qPCR

Primer name	Sequence
FABP4 forward	5′-AAATCACCGCAGACGACAGG-3′
FABP4 reverse	5′-GGCTCATGCCCTTTCATAAAC-3′
CEBPα forward	5′-CTGATTCTTGCCAAACTGAG-3′
CEBPα reverse	5′-GAGGAAGCTAAGACCCACTAC-3′
RRARγ forward	5′-CTTGACAGGAAAGACAACGG-3′
RRARγ reverse	5′-GCTTCTACGGATCGAAACTG-3′
β-Catenin forward	5′-GTTCGCCTTCATTATGGACTGCC-3′
β-Catenin reverse	5′-ATAGCACCCTGTTCCCGCAAAG-3′
OCN forward	5′-AGGGAGGATCAAGTCCCG-3′
OCN reverse	5′-GAACAGACTCCGGCGCTA-3′
ALP forward	5′-GTTGGGGGTGCCCACGGT-3′
ALP reverse	5′-CCTTGGACAGAGCCATGTATG-3′
Runx2 forward	5′-GAGGGCACAAGTTCTATCTGGA-3′
Runx2 reverse	5′-GGTGGTCCGCGATGATCTC-3′
β-Actin forward	5′-GGAGATTACTGCCCTGGCTCCTA-3′
β-Actin reverse	5′-GACTCATCGTACTCCTGCTTGCTG-3′

Huabio, Hangzhou, Zhejiang, China), runt-related transcription factor-2 (Runx2; diluted 1 : 1000, ET1612-47; Huabio, Hangzhou, Zhejiang, China), alkaline phosphatase (ALP; diluted 1 : 5000, ARG57422; Arigo, Taiwan, China), peroxisome proliferator-activated receptor gamma (PPARγ; diluted 1 : 1000, ARG55241; Arigo, Taiwan, China), and glyceraldehyde-3-phosphate dehydrogenase (GAPDH; diluted 1 : 5000, ET1601-4; Huabio, Hangzhou, Zhejiang, China) in tris-buffered saline Tween-20. Then, the membranes were washed and incubated with the corresponding secondary antibody at room temperature without light for 2 h. Then, the expression of proteins was detected using an Odyssey® CLX Imaging System (LI-COR Biosciences, Nebraska, USA) following the manufacturer's protocol.

In vivo studies

The animal experiments were approved by the Ethics Committee of Zhejiang Chinese Medical University (Hangzhou, China; approval no. 20190401-10) and carried out following the National Institutes of Health Guide for the Care and Use of Laboratory Animals. Forty male Sprague–Dawley rats of age 3 months (weighing ~ 500 g) were purchased from the Shanghai SLAC Laboratory Animals Ltd, Shanghai, China (license number SCXK(Hu)2017-0005). After a week of adaptive feeding, the rats were randomly divided into four groups (n = 10): (1) the control group, (2) the model group, (3) the GA group (treated with GA at a dosage of 50 mg kg^{-1} d^{-1} (ref. 29) *via* oral administration for 6 weeks), and (4) the Wnt/β-catenin pathway agonist-S8320 group (treated with S8320 at a dosage of 5 mg kg^{-1} d^{-1} (ref. 30) *via* intraperitoneal injection for 6 weeks). The rat models of SONFH were described previously.[31] In brief, on day 1, each rat was given a delayed injection of lipopolysaccharide (LPS; 0.2 mg kg^{-1}, Sigma-Aldrich, St Louis, USA) *via* the tail vein over 1 h, except for the control group, which was given a slow injection of an equal amount of saline *via* the tail vein. On days 2–4, the rats were given intraperitoneal injections of methylprednisolone (MPS; 100 mg kg^{-1}; Pfizer, NY, USA) once daily, followed by 40 mg kg^{-1} MPS three times a week between weeks 3 and 8, and the rats of the control group were intraperitoneally injected the same amount of normal saline at the same time. The rats were housed at a stationary room temperature of 20 ± 2 °C and 50–60% humidity for a 12 h light/dark cycle, according to 2 rats to a cage, and were provided with pure water and standard food access.

Biomechanical testing

The load-bearing capacity of the femoral heads was analysed by an axial compression tester (Bose Corp, Minnesota, USA). The axial compression tester was used to test the static loading of the femoral head at a speed of 0.5 mm min^{-1}. The appearance of the first mechanical turning point during loading deformation will define the load-bearing capacity.

Micro-CT scanning (μCT)

Femoral head samples from humans and rats were examined by μCT analysis. In brief, the samples were scanned by using a μCT scanner (Skyscan 1176, Bruker, Kontich, Belgium) with a resolution of 18 μm. Image reconstruction and analysis were performed using NRecon v1.6 (Bruker, Kontich, Belgium) and CTAn v1.9 (Bruker, Kontich, Belgium), respectively. The reconstructed images were employed for analyzing bone parameters, including bone mineral density (BMD), trabecular number (Tb·N), trabecular bone volume fraction (BV/TV), trabecular thickness (Tb·Th), trabecular separation (Tb·Sp) and structure model index (SMI).

Histology and histomorphometry

Human and rat femoral head sections were decalcified, embedded in paraffin, cut into 3-μm-thick slices, and stained with Alcian Blue Hematoxylin/Orange G (ABH/OG) for histological analysis as described previously.[32] Osteoblasts, adipocytes and trabecular morphology of the subchondral bone of the femoral head were assessed using light microscopy (Axioscope A1; Zeiss, Oberkochen, Germany) and the proportion of empty bone lacunae, the area and diameter of adipocytes and the area of trabecular bone were calculated.

ROS detection

For detection of ROS, freshly isolated human and rat femoral head tissues were rapidly frozen and cut into 5-μm-thick slices at optimized cutting temperatures and mounted on glass slides. A DHE-ROS assay kit (BB-470516; BestBio, Shanghai, China) was used according to the standard protocol to detect the ROS levels. In brief, frozen human and rat femoral head sections were stained with dihydroethidium (DHE) for 30 minutes in darkness. The positive expression of ROS was observed by fluorescence microscopy (X-Cite® 120Q; Lumen Dynamics, Newtown, New Jersey, USA) and quantified by the Image-Pro software (Media Cybernetics, Silver Spring, Maryland, USA).

Immunohistochemistry (IHC)

Human and rat femoral head sections were dewaxed and rehydrated before incubating for 4 h at 60 °C in 0.01 M citrate buffer (Solarbio, Beijing, China) for antigen retrieval. Next, the

sections were incubated with primary antibodies against β-catenin (diluted 1 : 500, 51067-2-AP; Proteintech, Chicago, USA), Runx2 (diluted 1 : 200, ET1612-47; Huabio, Hangzhou, Zhejiang, China), Osterix (OSX; diluted 1 : 200, ER1914-47; Huabio, Hangzhou, Zhejiang, China), PPARγ (diluted 1 : 200, ARG55241; Arigo, Taiwan, China), and FABP4 (diluted 1 : 200, ab92501; Abcam, Cambridge, UK) overnight at 4 °C. On the second day, after reacting with the secondary antibody (diluted 1 : 1000, 31234; Invitrogen, Carlsbad, California, USA) for 20 min at room temperature, a diaminobenzidine (DAB) solution was used to detect positive staining while counterstaining with hematoxylin was performed. A light microscope (Axioscope A1; Zeiss, Oberkochen, Germany) was employed to detect the positive staining at 200× magnification. Then the quantification was assessed by the Image-Pro software (Media Cybernetics, Silver Spring, Maryland, USA).

Statistical analysis

All data were expressed as mean ± standard deviation. One-way ANOVA was performed using the SPSS 20.0 software, followed by Dunnett's test. A P value <0.05 was considered to indicate statistical significance. All the experiments consisted of at least three replicates.

3. Results

Imbalance in the osteolipogenic homeostasis of the femoral head induced by excessive OS may contribute to the pathogenesis of SONFH

Fig. 1B displayed typical features of the SONFH specimen, where radiographs of SONFH exhibited fractured and cystic changes of the subchondral bone and collapsed areas of necrosis compared to the FNF specimen (Fig. 1A). A μCT analysis of the changes in bone mass revealed a significant reduction in the number of subchondral trabeculae in SONFH compared to FNF, accompanied by a myriad of fragmented trabeculae (Fig. 1C–F). Morphometric analyses of the μCT data demonstrated that the BMD, Tb·N, and Tb·Th of SONFH were lower than those of FNF, whereas Tb·Sp was conversely higher (P < 0.001) (Fig. 1G). To further observe the histopathological changes, the ABH/OG staining was performed which displayed abnormal cancellous bone, homogeneous necrotic material in the bone marrow, and a large number of fat vacuoles compared to the FNF specimen (P < 0.001) (Fig. 1H and I). The expression of the osteogenic-related protein (Runx2, OSX) was reduced in the SONFH bone tissue while the expression of the lipogenic-related protein (PPARγ, FABP4) was enhanced compared with the FNF specimen (Fig. 1J and K). To further elucidate the pathogenesis of SONFH, we performed ROS immunofluorescence staining and the results indicated that subchondral bone ROS levels were significantly higher in SONFH patients compared to FNF patients (P < 0.001) (Fig. 1L). These results suggested that an imbalance in osteolipogenic homeostasis of the femoral head caused by excess OS may be a mechanism for the pathogenesis of SONFH.

GA counteracted the pro-oxidative stress effects of Dex and maintained osteolipogenic homeostasis in MSCs

A CCK-8 assay was performed to analyze the proliferation of MSCs and the results indicated that 1 μM of Dex inhibited the proliferation of MSCs at 24 h, 48 h, and 72 h. In contrast, GA substantially counteracted the inhibitory effect of Dex upon the proliferation of MSCs in a dose-dependent manner. Notably, 80 μM GA exhibited the best proliferation promoting effect at 12 h, 24 h, and 48 h (Fig. 2A). Therefore, we used 80 μM GA in the following experiments. The gene expression of Runx2, OCN and ALP, osteogenesis-related markers, was reduced by Dex. In contrast, GA counteracted the inhibition and stimulated gene expression to a higher level (Fig. 2B–D). Furthermore, when MSCs were cultured in 1 μM Dex, the protein expression of ALP and Runx2 was reduced, and the inhibitory effect was rescued by GA supplementation (Fig. 2E). Moreover, the application of ALP staining to assess the early mineralization capacity of MSCs revealed that Dex reduced the mineralization capacity of MSCs, as evidenced by a pronounced decrease in ALP activity (P < 0.001). In contrast, GA restored the osteogenic capacity of MSCs when co-cultured with 1 μM Dex (P < 0.001) (Fig. 2F). The adipogenesis-related markers, C/EBPα, PPARγ and FABP4 were measured by RT-qPCR in MSCs treated with Dex and GA. As illustrated in Fig. 2G, the gene expression levels of PPARγ, C/EBPα and FABP4 were enhanced by Dex, while GA counteracted these enhancements. In addition, Dex increased the protein level of PPARγ in MSCs. However, the enhancement was counteracted by GA co-treatment (Fig. 2H). An adipogenesis assay suggested that Dex significantly stimulated adipogenesis in MSCs with a substantial amount of lipid vacuole formation (P < 0.001). In contrast, GA suppressed the facilitation of adipogenic differentiation of MSCs by Dex (Fig. 2I). In addition, based on the importance of OS on the differentiation fate of MSCs and our clinical results, we examined the levels of ROS and OS critical protein (NOX4) and showed that 1 μm Dex significantly increased the OS levels in MSCs, while GA partially counteracted this promotion (Fig. 2H and J). These results suggested that GA counteracted the pro-oxidative stress effects of Dex and maintained osteolipogenic homeostasis in MSCs.

GA may alleviate SONFH through the Wnt signaling pathway identified by network pharmacology

The PPI network represented the protein interactions of the GA targets and manifested that β-catenin plays an essential role (Fig. 3A). The topological analysis ultimately identified 7 key nodes containing β-catenin, which is the most critical target of the Wnt pathway (Fig. 3B). The results of GO were mainly associated with cell differentiation, cell proliferation and inflammatory pathways (Fig. 3C). The KEGG pathway enrichment analysis revealed that the Wnt signaling pathway was markedly enriched (Fig. 3D). The above results implied that GA is likely to be involved in regulating MSC differentiation of SONFH through the Wnt signaling pathway.

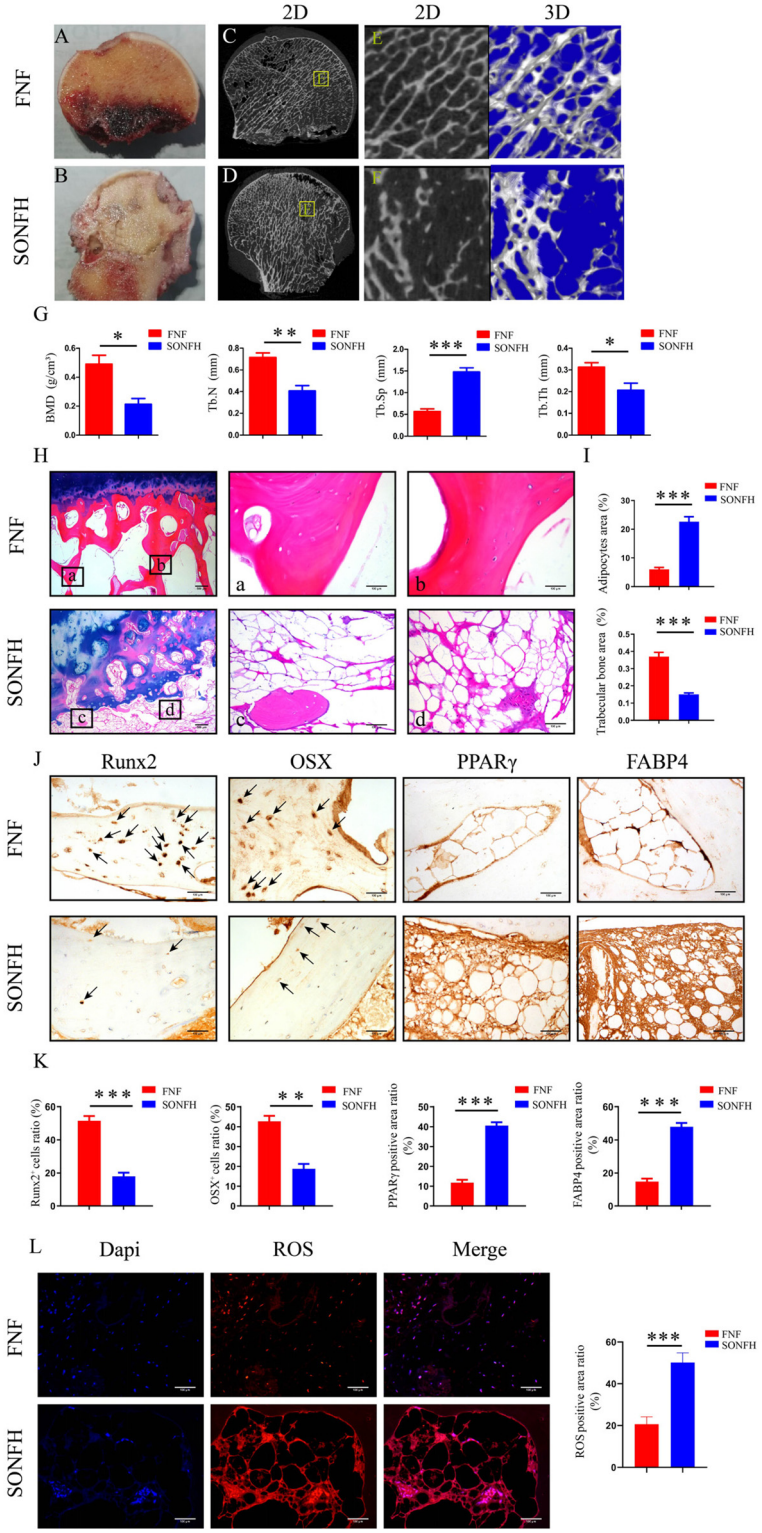

Fig. 1 Gross morphology, radiographs and histopathology images of human femoral head samples. (A and B) Gross morphology of FNF and SONFH femoral heads. (C–F) 2D and 3D μCT images of the femoral head. (G) Quantitative analysis of BMD, Tb·N, Tb·Sp and Tb·Th. (H) Histological images (ABH/OG) of the femoral head. (I) Histomorphometric analysis of ABH/OG staining. (J) IHC staining of the femoral head. (K) Quantitative analysis of IHC staining. (L) ROS staining of the femoral head. Data are expressed as mean ± SD, $^{*}P < 0.05$, $^{**}P < 0.01$, and $^{***}P < 0.001$ (*vs.* SONFH).

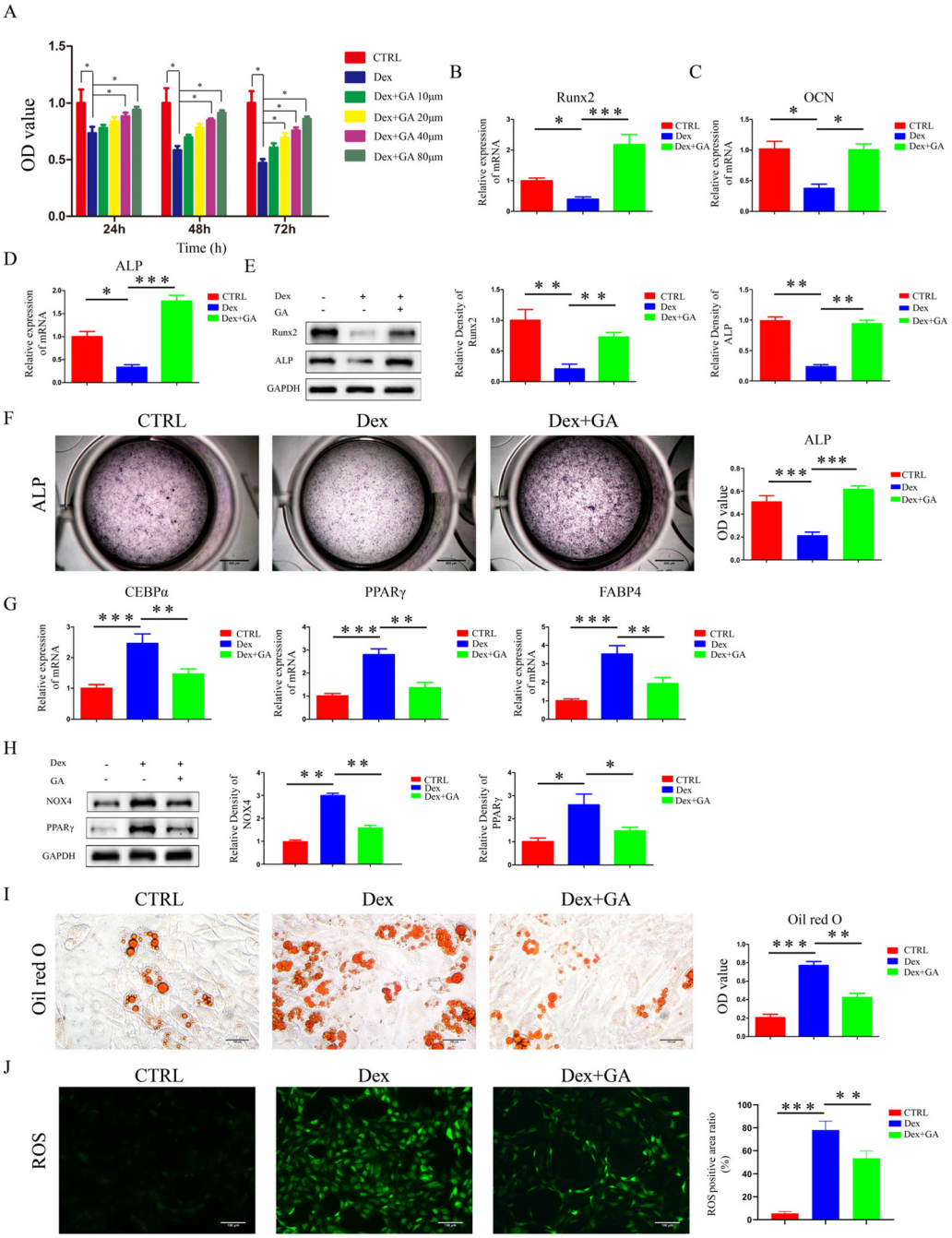

Fig. 2 GA counteracted the pro-oxidative stress effects of Dex and maintained osteolipogenic homeostasis in MSCs. (A) The proliferation capacity of MSCs treated with Dex and GA was evaluated by a CCK-8 assay. (B–D) Runx2, OCN, and ALP mRNA of MSCs treated with Dex and GA. (E) Runx2 and ALP protein levels of MSCs treated with Dex and GA. (F) ALP staining of MSCs incubated with Dex and GA for 14 days. (G) C/EBPα, PPARγ and FABP4 mRNA of MSCs treated with Dex and GA. (H) NOX4 and PPARγ protein levels of MSCs treated with Dex and GA. (I) Oil red O staining of MSCs incubated with Dex and GA for 21 days. (J) ROS staining of MSCs incubated with Dex and GA. The Dex concentration used in (B–J) was 1 μM and the GA concentration was 80 μM. Data are expressed as mean ± SD, $*P < 0.05$, $**P < 0.01$, $***P < 0.001$ (*vs.* Dex).

GA was similar to Wnt agonist in alleviating SONFH rats

The animal experimental flow is shown in Fig. 4A. We found that GA ameliorated the microstructure of the trabecular bone and histopathological changes in SONFH rats (ESI Fig. 2†) while increasing the expression of osteogenic-related protein and inhibiting the expression of the lipogenic-related protein (ESI Fig. 3†). The results of network pharmacology suggested that GA may alleviate SONFH by activating the Wnt/β-catenin pathway. We then performed the IHC assay for β-catenin (the most crucial protein in the Wnt/β-catenin pathway and a critical node in the PPI network) in human samples and demon-

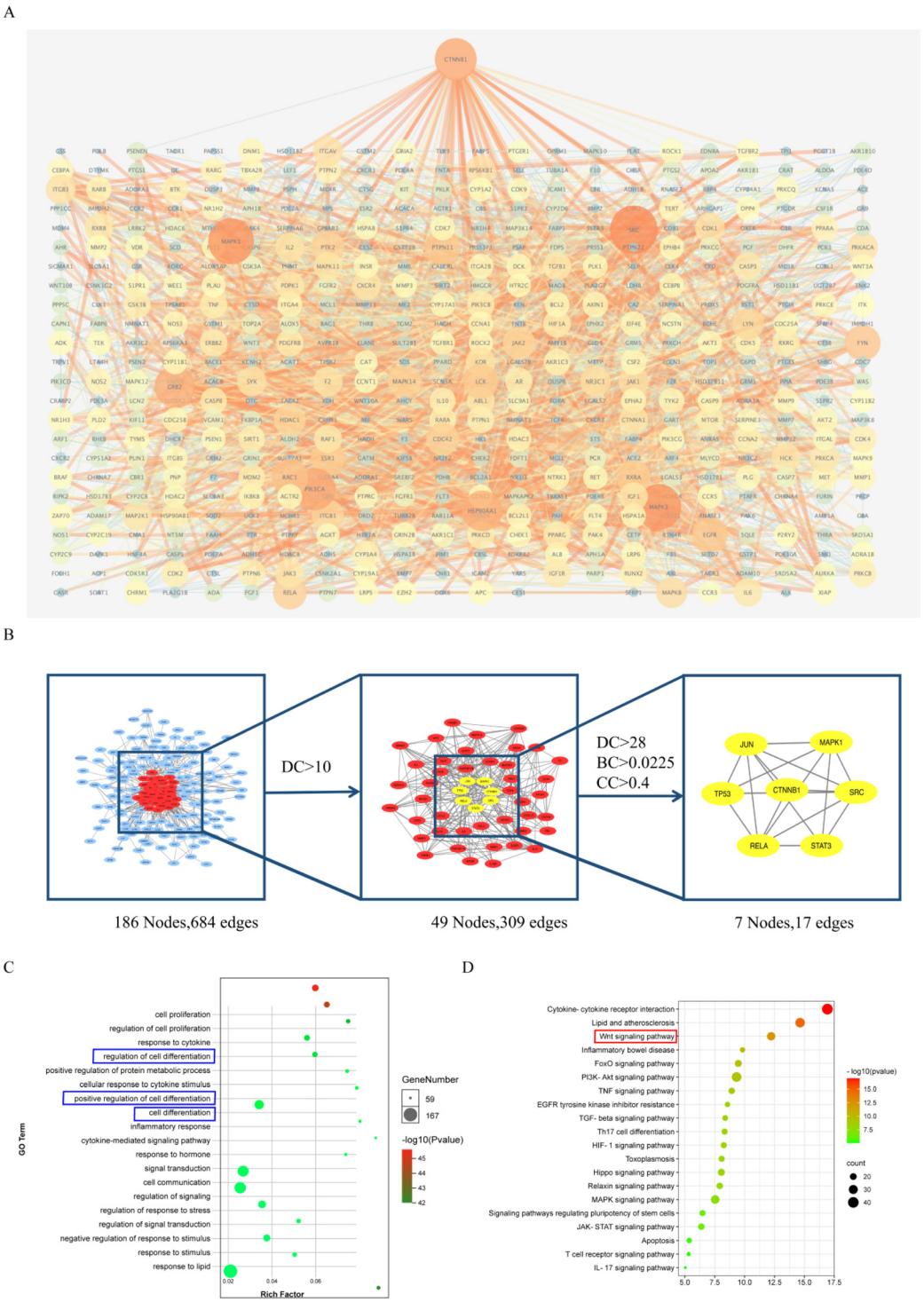

Fig. 3 The integration strategy of network pharmacology in GA alleviating SONFH. (A) PPI network of GA targets. (B) Topology analysis. (C) Bubble chart of the GO enrichment analysis. (D) Bubble chart of the KEGG pathway analysis. CTNNB1, the gene name encoding β-catenin.

strated that the expression level of β-catenin was lower in SONFH samples than in FNF samples (Fig. 4B). Thus, it is reasonable to speculate that GA could potentially treat SONFH by activating the Wnt/β-catenin pathway. To verify this hypothesis, the efficacy of the Wnt agonist-S8320 treatment group was compared with the GA treatment group in our animal experiments. As we expected, the S8320 and GA-treated groups exhibited promising therapeutic efficacy compared with the model group. The general appearance of the femoral head in the GA and S8320 treatment group was improved compared to the abnormal dark red appearance of the rats in the model group (Fig. 4C). Simultaneously, the mechanical testing exhibi-

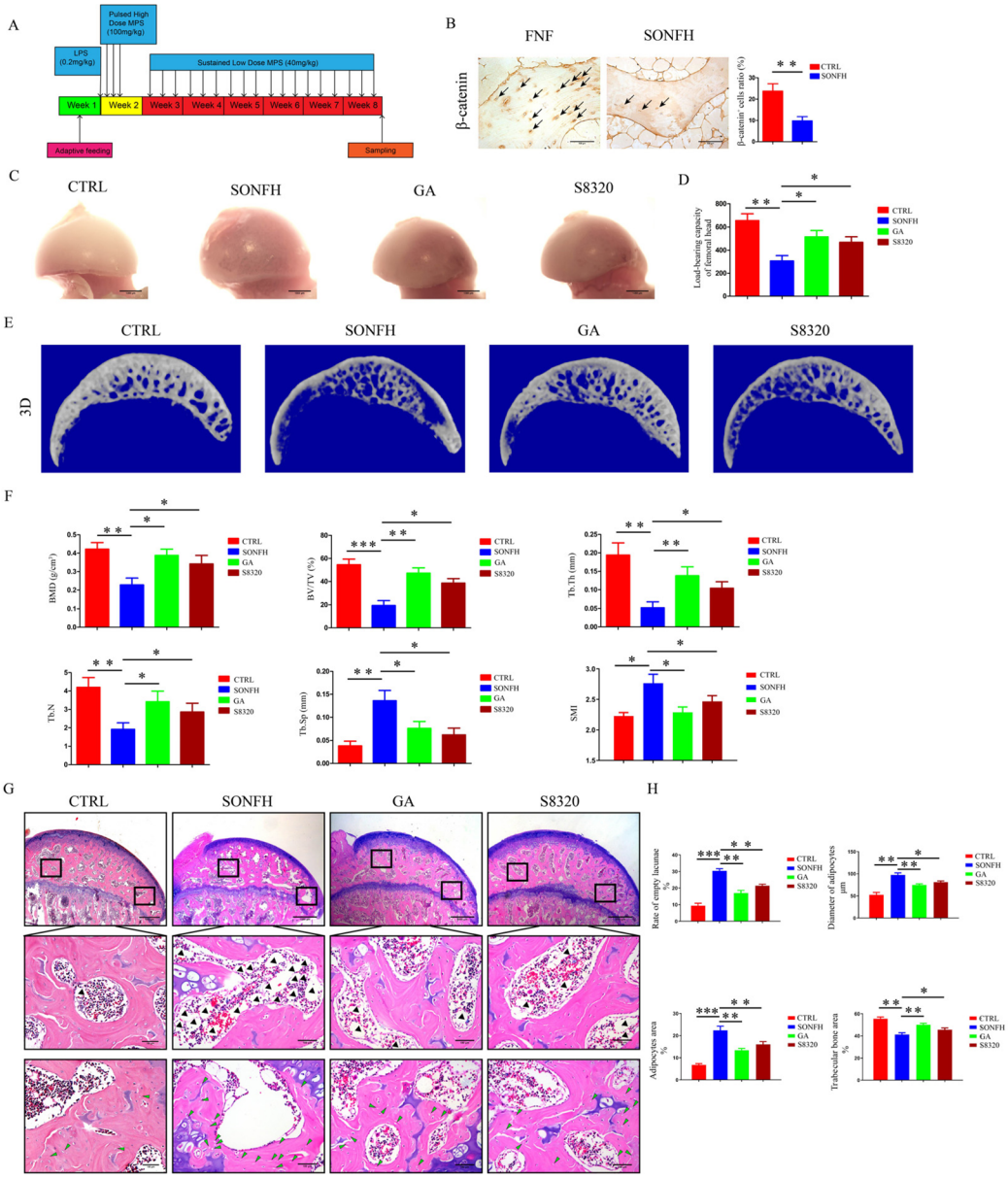

Fig. 4 GA has similarities with the Wnt agonist in attenuating SONFH rats. (A) The schematic diagram of the *in vivo* modeling procedure. The GA group (treated with GA at a dosage of 50 mg kg^{-1} d^{-1} *via* oral administration for 6 weeks), the Wnt/β-catenin pathway agonist-S8320 group (treated with S8320 at a dosage of 5 mg kg^{-1} d^{-1} *via* intraperitoneal injection for 6 weeks). (B) IHC staining and the quantitative analysis of the β-catenin of human femoral head samples. (C) Gross morphology of rat femoral head samples. (D) The load-bearing capacity of rat femoral head samples. (E) μCT scanning images of rat femoral head samples. (F) Quantitative analysis of BMD, BV/TV, Tb·Th, Tb·N, Tb·Sp and SMI. (G) Histological images (ABH/OG) of rat femoral head samples. (H) Histomorphometric analysis of ABH/OG staining. The adipocytes are indicated by black arrows and the empty lacunae are indicated by green arrows. Data are expressed as mean ± SD, $^{*}P < 0.05$, $^{**}P < 0.01$, and $^{***}P < 0.001$ (*vs.* SONFH).

ted that the load-bearing capacity of the femoral head in the GA and S8320 groups was prominently superior to that of the SONFH group (Fig. 4D). Moreover, GA and S8320 ameliorated the critical microstructural parameters, including elevated BMD, BV/TV, Tb·Th, and Tb·N, as well as reduced Tb·Sp and SMI (Fig. 4E and F). Besides, ABH/OG staining indicated the femoral head in the model group exhibited numerous nuclear divisions in the trabeculae and innumerable voids accompanied by a large number of fat vacuoles. In contrast, the ratio of empty lacunae, the diameter and area of adipocytes, and the area of trabecular bone were improved after GA and S8320 treatment (Fig. 4G and H). Furthermore, the IHC of osteogenic and adipogenic-associated proteins revealed results similar to the S8320 and GA treatment groups; both increased the expression of the osteogenic protein (Runx2) while suppressing the expression of lipogenic proteins (PPARγ and FABP4) (Fig. 5A and C–E). Notably, the expression level of β-catenin was diminished in the model group compared to the

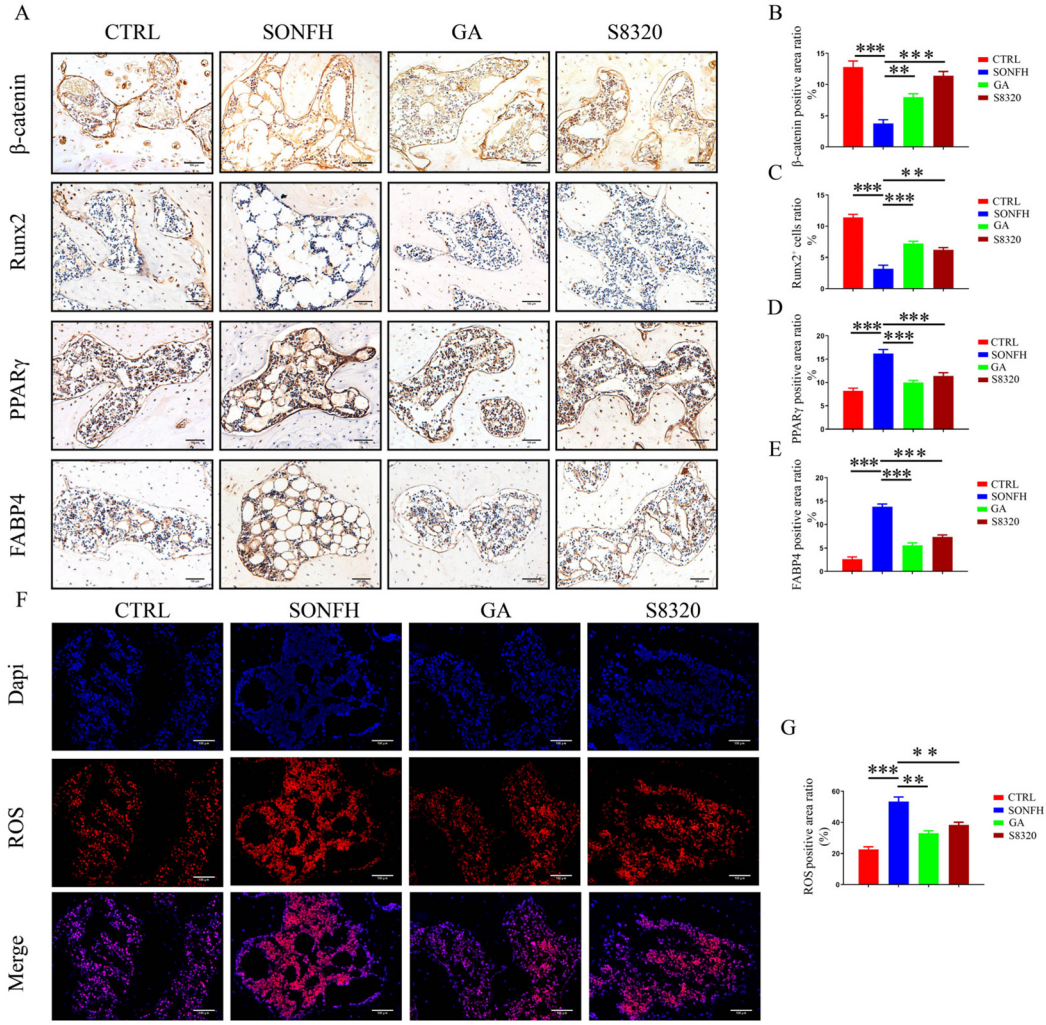

Fig. 5 Both GA and the Wnt agonist-S8320 reduced ROS levels, accelerated osteogenic differentiation and restrained lipogenic differentiation in SONFH rats. (A) IHC staining of β-catenin, Runx2, PPARγ and FABP4 in different groups of rats. (B–E) Quantitative analysis of β-catenin, Runx2, PPARγ and FABP4. (F) ROS staining of different groups of rats. (G) Quantitative analysis of ROS. Data are expressed as mean ± SD, $^{**}P < 0.01$ and $^{***}P < 0.001$ (*vs.* SONFH).

control group, whereas both the treatment of GA and S8320 could rescue this repression and facilitate the expression of β-catenin to higher levels (Fig. 5A and B). Based on the results of the clinical samples and the association of OS with MSC differentiation, we performed ROS immunofluorescence test and showed that, consistent with the human samples, the ROS levels were significantly increased in SONFH rats ($P < 0.001$), while both GA and S8320 could reduce OS levels (Fig. 5F and G). These data confirmed the similarity of GA and S8320 in mitigating SONFH rats, reducing OS levels, and thereby promoting osteogenesis and inhibiting lipogenesis.

GA decreases OS levels in MSCs by activating the Wnt/β-catenin pathway and maintains their osteolipogenic differentiation homeostasis

In an attempt to clarify whether GA reduced OS levels by activating the Wnt/β-catenin pathway and thus regulated osteolipogenic differentiation in MSCs, we conducted *in vitro* mechanistic studies using the agonist-S8320 and the inhibitor-S8761 of the Wnt/β-catenin pathway. As mentioned previously, GA partially counteracted the elevated OS levels caused by Dex. In addition, S8320 exhibited similar effects to GA but S8761 eliminated the protective effect of GA against Dex-induced OS elevation, both in terms of ROS and NOX4 levels (Fig. 6A, B and G). When MSCs were cultured in 1 μM Dex, the gene and protein levels of β-catenin were decreased. This inhibition was reversed by supplemental GA (ESI Fig. 4†). Regarding osteogenesis, RT-qPCR results showed that when Dex-treated MSCs were incubated further with GA, 100 nM S8761 diminished the up-regulation of Runx2, OCN, ALP and β-catenin (Fig. 6C). The result of WB also exhibited a similar trend, with the Runx2, ALP and β-catenin protein expression levels reduced after 100 nM S8761 treatment (Fig. 6D). Moreover, the results of ALP staining displayed that S8761 abolished the protective function

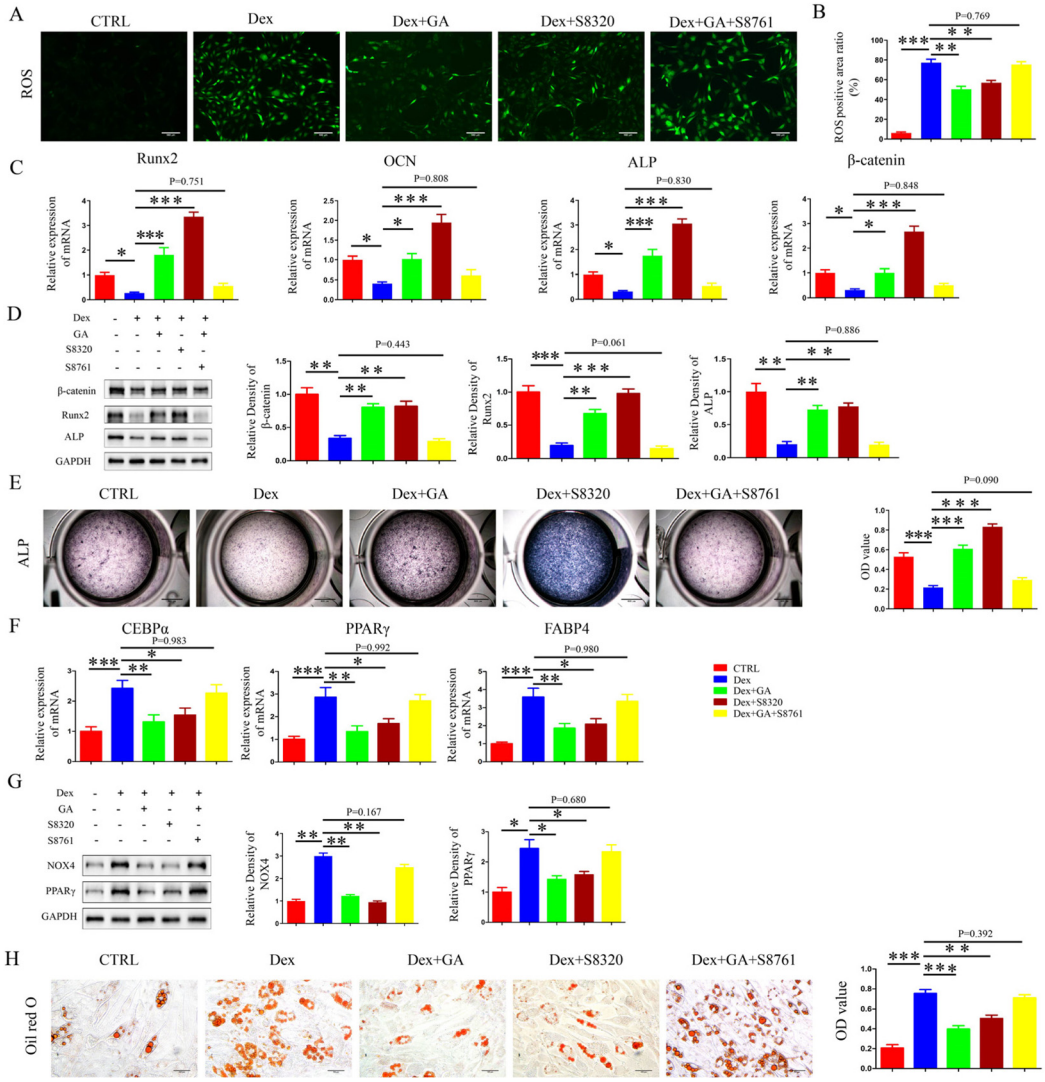

Fig. 6 GA reduced OS levels in MSCs *via* activation of the Wnt/β-catenin pathway, thereby maintaining their osteolipogenic differentiation homeostasis. (A) ROS staining in different groups. (B) Quantitative analysis of ROS. (C) The mRNA level of Runx2, OCN, ALP and β-catenin. (D) The protein level of β-catenin, Runx2 and ALP. (E) ALP staining for 14 days. (F) The mRNA level of C/EBPα, PPARγ, and FABP4. (G) The protein level of NOX4 and PPARγ. (H) Oil red O staining for 21 days. The concentration of Dex used in (A–H) was 1 μM, the concentration of GA was 80 μM, the concentration of S8320 was 10 μM and the concentration of S8761 was 100 nM. Data are expressed as mean ± SD, $*P < 0.05$, $**P < 0.01$, $***P < 0.001$ (*vs.* Dex).

of GA on Dex-induced loss of extracellular mineralization ($P < 0.001$) (Fig. 6E). Surprisingly, S8320 displayed efficacy similar to GA in promoting the osteogenic differentiation of MSCs, regardless of the gene level, the protein level or ALP staining (Fig. 6C–E). As for adipogenic differentiation, RT-qPCR and WB revealed a pronounced reduction in the up-regulation of PPARγ, CEBPα and FABP4 by 100 nM S8761 when MSCs were incubated with Dex and GA (Fig. 6F and G). Furthermore, the results of Oil red O staining demonstrated that S8761 abrogated the preventive function of GA on Dex-induced adipogenesis of MSCs (Fig. 6H). However, S8320 exhibited similar efficacy to GA in repressing the Dex-induced enhancement of PPARγ, CEBPα, and FABP4 gene and protein levels, thereby suppressing lipid differentiation of MSCs (Fig. 6F–H). These data seemed to highlight that GA reduced the level of OS in MSCs by activating the Wnt/β-catenin pathway, thereby maintaining their osteolipogenic differentiation homeostasis and ultimately treating SONFH.

4. Discussion

We identified SONFH patients with the manifestation of decreased bone mass, altered bone microarchitecture, and increased fat accumulation in the medullary cavity, which was consistent with the findings of previous studies.[9,33] In addition, we found significantly increased OS levels of subchondral bone in SONFH patients, which may also be a contributing factor.[34] Currently, there are three primary modeling methods for SONFH: MPS alone, MPS combined with allo-

geneic serum and LPS combined with MPS. We found that LPS combined with MPS modeling was highly mimetic of early-stage SONFH patients using histopathological comparisons.

Recent studies have shown that OS is an essential pathophysiological mechanism in SONFH,[34,35] and excessive ROS caused by high doses of GCs exacerbates the OS microenvironment in the necrotic zone.[36] MSCs normally have low levels of intracellular ROS, which regulate MSC differentiation and proliferation.[37] Excess OS can alter the differentiation fate of MSCs, inhibit osteogenic differentiation and promote lipogenic differentiation.[38] Our results demonstrated that the imbalance in the differentiation fate of MSCs caused by excess OS might be one of the pathogenic mechanisms of SONFH.

As an evolutionarily conserved signaling pathway, the Wnt pathway has been extensively investigated for its critical role in MSC renewal, proliferation and differentiation.[39] It plays a crucial part in regulating bone homeostasis by promoting osteoblast differentiation while inhibiting the differentiation of MSCs towards adipocytes,[40,41] which were closely related to the occurrence and development of SONFH. The Wnt pathway can regulate the OS levels, but the relationship between them needs further study. It has been shown that activation of the Wnt pathway enhances NOX4 protein expression and ROS production.[42–45] However, other studies have also demonstrated that activation of the Wnt pathway weakens the production of cellular lipid ROS[46] and attenuates the increase in ROS induced by OS damage in mitochondria *via* trans-nuclear action.[47] Our study demonstrated that activation of the Wnt pathway can inhibit NOX4 protein expression and ROS levels in MSCs, resulting in reduced OS levels.

GA is a triterpenoid saponin glycoside known as the most medically efficacious component of the licorice plant. Studies have shown that GA has antioxidant pharmacological effects. Specifically, GA can reduce OS by inhibiting the MAPK and NF-κB pathways and activating the AMPK/NRF2 pathway.[48] In addition, GA has been shown to enhance antioxidant capacity and reduce free radical-induced lipid peroxidation in mice.[49] Similar to their findings, the results of the present study suggested that GA could reduce OS levels in MSCs and the subchondral bone of the rat femoral head. In addition, recent literature has reported that GA is capable of promoting osteoblast differentiation and thus is beneficial for the therapeutic efficacy in the management of orthopaedic conditions such as fractures,[24] osteoarthritis[29] and postmenopausal osteoporosis.[50] In addition, studies have shown that GA suppressed the early stage of adipogenesis by restraining the expression of lipogenic transcription factors *in vitro*.[26] As shown in Fig. 7, the results of this study demonstrated that GA activated the Wnt/β-catenin signaling pathway, thereby reducing the elevation of NOX4 expression induced by excessive GCs, thus inhibiting oxidative damage in MSCs, maintaining their osteolipogenic homeostasis and ultimately treating SONFH.

Inevitably, there are some limitations to this study. We were the first to suggest that GA reduces OS levels through the activation of the Wnt/β-catenin pathway and thereby regulates the fate of osteolipogenic differentiation in MSCs. Still, the exact

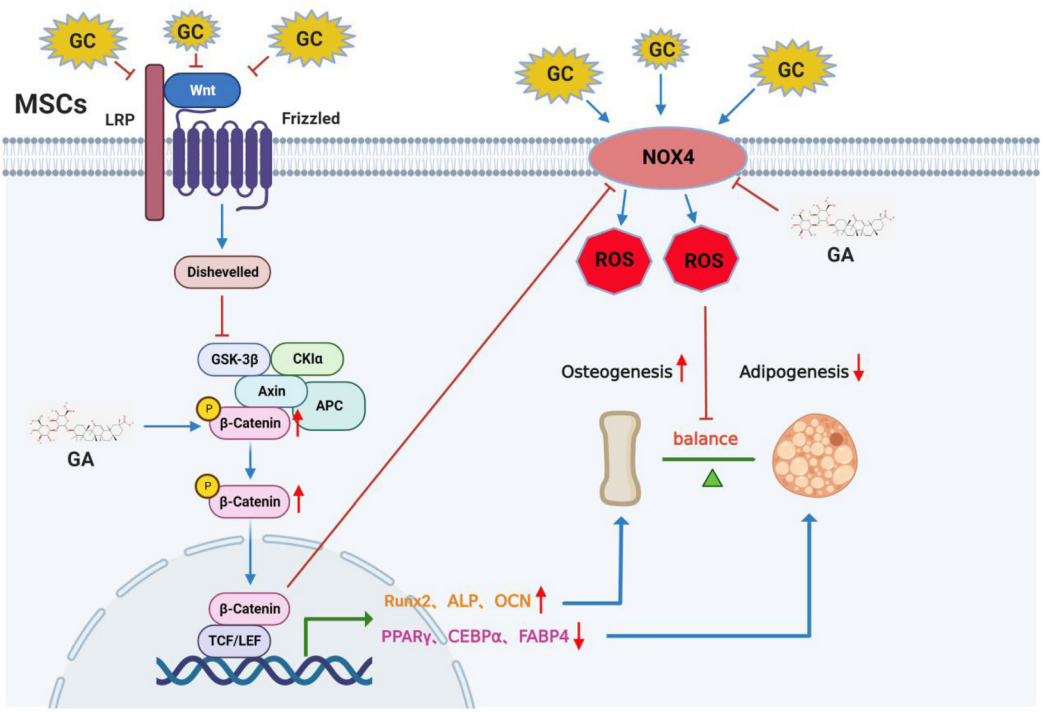

Fig. 7 Schematic illustration of the potential protective effects of GA in SONFH development. GA can reduce the level of OS induced by excessive GCs through the activation of the Wnt/β-catenin signaling pathway, thereby maintaining the osteolipogenic homeostasis of MSCs.

targets of GA regulation of the Wnt pathway and the relationship with the upstream and downstream proteins need further investigation. Moreover, the duration of our intervention was short and future studies will extend the treatment period to observe the efficacy of GA in treating SONFH in the long term. At the same time, a prophylactic group, where GA treatment is given after the first MPS injection, will be added to explore the preventive effect of GA on SONFH.

5. Conclusion

Our study has illustrated, for the first time, that GC-induced SONFH could be mitigated by GA both *in vivo* and *in vitro*. The protective efficacy is mediated by activating the Wnt/β-catenin pathway, which reduces the OS levels induced by excessive GCs, thereby enhancing osteogenic differentiation, attenuating lipogenic differentiation of MSCs, and ultimately maintaining osteolipogenic homeostasis. In the current study, we have uncovered a formerly uncharted role of GA and unveiled its underlying pharmacotherapeutic use against GC-induced SONFH.

Abbreviations

GA	Glycyrrhizic acid
SONFH	Steroid-induced necrosis of the femoral head
FNF	Femoral neck fractures
LPS	Lipopolysaccharide
MPS	Methylprednisolone
OS	Oxidative stress
Dex	Dexamethasone
NOX4	Nicotinamide adenine dinucleotide phosphate oxidase-4
ROS	Reactive oxygen species
MSCs	Mesenchymal stem cells
BMSCs	Bone marrow mesenchymal stem cells
TCM	Traditional Chinese medicine
PPI	Protein–protein interaction
GO	Gene ontology
KEGG	Kyoto Encyclopedia of Genes and Genomes
Runx2	Runt-related transcription factor-2
OSX	Osterix
ALP	Alkaline phosphatase
C/EBPα	CCAAT/enhancer binding proteins alpha
PPARγ	Peroxisome proliferator-activated receptor gamma
FABP4	Fatty acid binding protein-4
ABH/OG	Alcian Blue Hematoxylin/Orange G
OCN	Osteocalcin

Author contributions

The authors confirm the contribution to the paper as follows: study conception and design: Bangjian He, Peijian Tong, and Hongting Jin; experiment and data collection: Huihui Xu, Qinghe Zeng, Liang Fang, Jiali Chen, Houfu Ling, Hanting Xia, Qinwen Ge, and Congzi Wu; analysis and interpretation of results: Huihui Xu, Qinghe Zeng, Liang Fang, Kaiao Zou, Xu Wang, and Pinger Wang; draft manuscript preparation: Huihui Xu, Qinghe Zeng, Wenhua Yuan, Rui Dong, Songfeng Hu, and Luwei Xiao. All authors reviewed the results and approved the final version of the manuscript.

Conflicts of interest

There are no conflicts of interest to declare.

Acknowledgements

This work has been partially supported by the Natural Science Foundation of China (grant no. 82074469, 81873325 and 82004389), the Zhejiang grants funded by the Provincial Natural Science Foundation of China (grant no. Y21H270035), and the State Administration of Traditional Chinese Medicine of Zhejiang Province (grant no. 2021ZA136 and 2021ZZ014).

References

1 V. C. Bose and B. D. Baruah, Resurfacing arthroplasty of the hip for avascular necrosis of the femoral head: a minimum follow-up of four years, *J. Bone Jt. Surg., Br. Vol.*, 2010, **92**, 922–928.
2 J. Moya-Angeler, A. L. Gianakos, J. C. Villa, A. Ni and J. M. Lane, Current concepts on osteonecrosis of the femoral head, *World J. Orthop.*, 2015, **6**, 590–601.
3 D. Zhao, F. Zhang, B. Wang, B. Liu, L. Li, S. Y. Kim, S. B. Goodman, P. Hernigou, Q. Cui, W. C. Lineaweaver, J. Xu, W. R. Drescher and L. Qin, Guidelines for clinical diagnosis and treatment of osteonecrosis of the femoral head in adults (2019 version), *J. Orthop. Translat.*, 2020, **21**, 100–110.
4 T. Kubo, K. Ueshima, M. Saito, M. Ishida, Y. Arai and H. Fujiwara, Clinical and basic research on steroid-induced osteonecrosis of the femoral head in Japan, *J. Orthop. Sci.*, 2016, **21**, 407–413.
5 A. Agarwal, B. Rochwerg, R. A. Siemieniuk, T. Agoritsas, F. Lamontagne, L. Askie, L. Lytvyn, Y. S. Leo, H. Macdonald, L. Zeng, W. Amin, E. Burhan, F. J. Bausch, C. S. Calfee, M. Cecconi, D. Chanda, B. Du, H. Geduld, P. Gee, N. Harley, M. Hashimi, B. Hunt, S. K. Kabra, S. Kanda, Y. J. Kim, N. Kissoon, A. Kwizera, I. Mahaka, H. Manai, G. Mino, E. Nsutebu, J. Preller, N. Pshenichnaya, N. Qadir, S. Sabzwari, R. Sarin, M. Shankar-Hari, M. Sharland, Y. Shen, S. S. Ranganathan, J. P. Souza, M. Stegemann, A. De Sutter, S. Ugarte, S. Venkatapuram, V. Q. Dat, D. Vuyiseka, A. Wijewickrama, B. Maguire, D. Zeraatkar, J. J. Bartoszko, L. Ge, R. Brignardello-Petersen, A. Owen, G. Guyatt, J. Diaz, L. Kawano-Dourado,

M. Jacobs and P. O. Vandvik, A living WHO guideline on drugs for covid-19, *Br. Med. J.*, 2020, **370**, m3379.

6 J. Wang, Y. Ma, Y. Long and Y. Chen, Extracellular Vesicle Derived From Mesenchymal Stem Cells Have Bidirectional Effects on the Development of Lung Cancer, *Front. Oncol.*, 2022, **12**, 914832.

7 J. Li, N. Zhang, X. Huang, J. Xu, J. C. Fernandes, K. Dai and X. Zhang, Dexamethasone shifts bone marrow stromal cells from osteoblasts to adipocytes by C/EBPalpha promoter methylation, *Cell Death Dis.*, 2013, **4**, e832.

8 L. Han, B. Wang, R. Wang, S. Gong, G. Chen and W. Xu, The shift in the balance between osteoblastogenesis and adipogenesis of mesenchymal stem cells mediated by glucocorticoid receptor, *Stem Cell Res. Ther.*, 2019, **10**, 377.

9 M. T. Houdek, C. C. Wyles, B. D. Packard, A. Terzic, A. Behfar and R. J. Sierra, Decreased Osteogenic Activity of Mesenchymal Stem Cells in Patients With Corticosteroid-Induced Osteonecrosis of the Femoral Head, *J. Arthroplasty*, 2016, **31**, 893–898.

10 S. Xiang, Z. Li and X. Weng, The role of lncRNA RP11-154D6 in steroid-induced osteonecrosis of the femoral head through BMSC regulation, *J. Cell. Biochem.*, 2019, **120**, 18435–18445.

11 Y. J. Sung, T. Y. Kao, C. L. Kuo, C. C. Fan, A. N. Cheng, W. C. Fang, H. Y. Chou, Y. K. Lo, C. H. Chen, S. S. Jiang, I. S. Chang, C. H. Hsu, J. C. Lee and A. Y. Lee, Mitochondrial Lon sequesters and stabilizes p53 in the matrix to restrain apoptosis under oxidative stress via its chaperone activity, *Cell Death Dis.*, 2018, **9**, 697.

12 H. Sies and D. P. Jones, Reactive oxygen species (ROS) as pleiotropic physiological signalling agents, *Nat. Rev. Mol. Cell Biol.*, 2020, **21**, 363–383.

13 M. Vernier, C. R. Dufour, S. McGuirk, C. Scholtes, X. Li, G. Bourmeau, H. Kuasne, M. Park, J. St-Pierre, E. Audet-Walsh and V. Giguere, Estrogen-related receptors are targetable ROS sensors, *Genes Dev.*, 2020, **34**, 544–559.

14 J. P. He, X. Feng, J. F. Wang, W. G. Shi, H. Li, S. Danilchenko, A. Kalinkevich and M. Zhovner, Icariin prevents bone loss by inhibiting bone resorption and stabilizing bone biological apatite in a hindlimb suspension rodent model, *Acta Pharmacol. Sin.*, 2018, **39**, 1760–1767.

15 H. H. Xu, S. M. Li, R. Xu, L. Fang, H. Xu and P. J. Tong, Predication of the underlying mechanism of Bushenhuoxue formula acting on knee osteoarthritis via network pharmacology-based analyses combined with experimental validation, *J. Ethnopharmacol.*, 2020, **263**, 113217.

16 B. Fang, Y. Li, C. Chen, Q. Wei, J. Zheng, Y. Liu, W. He, D. Lin, G. Li, Y. Hou and L. Xu, Huo Xue Tong Luo capsule ameliorates osteonecrosis of femoral head through inhibiting lncRNA-Miat, *J. Ethnopharmacol.*, 2019, **238**, 111862.

17 G. Jia, X. Jiang, Z. Li, X. Ding, L. Lei, S. Xu and N. Gao, Decoding the Mechanism of Shen Qi Sha Bai Decoction in Treating Acute Myeloid Leukemia Based on Network Pharmacology and Molecular Docking, *Front. Cell Dev. Biol.*, 2021, **9**, 796757.

18 B. Guo, C. Zhao, C. Zhang, Y. Xiao, G. Yan, L. Liu and H. Pan, Elucidation of the anti-inflammatory mechanism of Er Miao San by integrative approach of network pharmacology and experimental verification, *Pharmacol. Res.*, 2022, **175**, 106000.

19 A. L. Hopkins, Network pharmacology: the next paradigm in drug discovery, *Nat. Chem. Biol.*, 2008, **4**, 682–690.

20 X. Feng, L. Ding and F. Qiu, Potential drug interactions associated with glycyrrhizin and glycyrrhetinic acid, *Drug Metab. Rev.*, 2015, **47**, 229–238.

21 Z. G. Sun, T. T. Zhao, N. Lu, Y. A. Yang and H. L. Zhu, Research Progress of Glycyrrhizic Acid on Antiviral Activity, *Mini-Rev. Med. Chem.*, 2019, **19**, 826–832.

22 X. Wang, H. Zhang, L. Chen, L. Shan, G. Fan and X. Gao, Liquorice, a unique "guide drug" of traditional Chinese medicine: a review of its role in drug interactions, *J. Ethnopharmacol.*, 2013, **150**, 781–790.

23 C. Y. Wang, T. C. Kao, W. H. Lo and G. C. Yen, Glycyrrhizic acid and 18beta-glycyrrhetinic acid modulate lipopolysaccharide-induced inflammatory response by suppression of NF-kappaB through PI3K p110delta and p110gamma inhibitions, *J. Agric. Food Chem.*, 2011, **59**, 7726–7733.

24 J. Bai, J. Xu, K. Hang, Z. Kuang, L. Ying, C. Zhou, L. Ni, Y. Wang and D. Xue, Glycyrrhizic Acid Promotes Osteogenic Differentiation of Human Bone Marrow Stromal Cells by Activating the Wnt/beta-Catenin Signaling Pathway, *Front. Pharmacol.*, 2021, **12**, 607635.

25 H. S. Cheng, H. P. Yaw, S. H. Ton, S. M. Choy, J. M. Kong and K. Abdul Kadir, Glycyrrhizic acid prevents high calorie diet-induced metabolic aberrations despite the suppression of peroxisome proliferator-activated receptor gamma expression, *Nutrition*, 2016, **32**, 995–1001.

26 M. Yamamoto, Y. Nagasawa and K. Fujimori, Glycyrrhizic acid suppresses early stage of adipogenesis through repression of MEK/ERK-mediated C/EBPbeta and C/EBPdelta expression in 3T3-L1 cells, *Chem.-Biol. Interact.*, 2021, **346**, 109595.

27 W. Zhu, M. Guo, W. Yang, M. Tang, T. Chen, D. Gan, D. Zhang, X. Ding, A. Zhao, P. Zhao, W. Yan and J. Zhang, CD41-deficient exosomes from non-traumatic femoral head necrosis tissues impair osteogenic differentiation and migration of mesenchymal stem cells, *Cell Death Dis.*, 2020, **11**, 293.

28 W. Huang, S. Jin, W. Yang, S. Tian, C. Meng, H. Deng and H. Wang, Protective effect of Agrimonia pilosa polysaccharides on dexamethasone-treated MC3T3-E1 cells via Wnt/beta-Catenin pathway, *J. Cell. Mol. Med.*, 2020, **24**, 2169–2177.

29 R. H. Jiang, J. J. Xu, D. C. Zhu, J. F. Li, C. X. Zhang, N. Lin and W. Y. Gao, Glycyrrhizin inhibits osteoarthritis development through suppressing the PI3K/AKT/NF-kappaB signaling pathway in vivo and in vitro, *Food Funct.*, 2020, **11**, 2126–2136.

30 Y. Ma, X. Lv, J. He, T. Liu, S. Wen and L. Wang, Wnt agonist stimulates liver regeneration after small-for-size

liver transplantation in rats, *Hepatol. Res.*, 2016, **46**, E154–E164.

31 H. H. Xu, S. M. Li, L. Fang, C. J. Xia, P. Zhang, R. Xu, Z. Y. Shi, Z. Zou, Q. W. Ge, P. Wang, P. J. Tong and H. T. Jin, Platelet-rich plasma promotes bone formation, restrains adipogenesis and accelerates vascularization to relieve steroids-induced osteonecrosis of the femoral head, *Platelets*, 2020, 1–10, DOI: 10.1080/09537104.2020.1810221.

32 H. Xu, R. Dong, Q. Zeng, L. Fang, Q. Ge, C. Xia, P. Zhang, S. Lv, Z. Zou, P. Wang, J. Li, H. Ruan, S. Hu, C. Wu, H. Jin and P. Tong, Col9a2 gene deletion accelerates the degeneration of intervertebral discs, *Exp. Ther. Med.*, 2022, **23**, 207.

33 C. Huang, Z. Wen, J. Niu, S. Lin and W. Wang, Steroid-Induced Osteonecrosis of the Femoral Head: Novel Insight Into the Roles of Bone Endothelial Cells in Pathogenesis and Treatment, *Front. Cell Dev. Biol.*, 2021, **9**, 777697.

34 K. Chen, Y. Liu, J. He, N. Pavlos, C. Wang, J. Kenny, J. Yuan, Q. Zhang, J. Xu and W. He, Steroid-induced osteonecrosis of the femoral head reveals enhanced reactive oxygen species and hyperactive osteoclasts, *Int. J. Biol. Sci.*, 2020, **16**, 1888–1900.

35 G. Deng, K. Niu, F. Zhou, B. Li, Y. Kang, X. Liu, J. Hu, B. Li, Q. Wang, C. Yi and Q. Wang, Treatment of steroid-induced osteonecrosis of the femoral head using porous Se@SiO_2 nanocomposites to suppress reactive oxygen species, *Sci. Rep.*, 2017, **7**, 43914.

36 T. McGarry, M. Biniecka, D. J. Veale and U. Fearon, Hypoxia, oxidative stress and inflammation, *Free Radicals Biol. Med.*, 2018, **125**, 15–24.

37 M. T. Houdek, C. C. Wyles, M. S. Collins, B. M. Howe, A. Terzic, A. Behfar and R. J. Sierra, Stem Cells Combined With Platelet-rich Plasma Effectively Treat Corticosteroid-induced Osteonecrosis of the Hip: A Prospective Study, *Clin. Orthop. Relat. Res.*, 2018, **476**, 388–397.

38 F. Atashi, A. Modarressi and M. S. Pepper, The role of reactive oxygen species in mesenchymal stem cell adipogenic and osteogenic differentiation: a review, *Stem Cells Dev.*, 2015, **24**, 1150–1163.

39 Y. Sun, Y. Yuan, W. Wu, L. Lei and L. Zhang, The effects of locomotion on bone marrow mesenchymal stem cell fate: insight into mechanical regulation and bone formation, *Cell Biosci.*, 2021, **11**, 88.

40 W. A. Bullock and A. G. Robling, WNT-mediated Modulation of Bone Metabolism: Implications for WNT Targeting to Treat Extraskeletal Disorders, *Toxicol. Pathol.*, 2017, **45**, 864–868.

41 Y. Li, D. Jin, W. Xie, L. Wen, W. Chen, J. Xu, J. Ding and D. Ren, PPAR-gamma and Wnt Regulate the Differentiation of MSCs into Adipocytes and Osteoblasts Respectively, *Curr. Stem Cell Res. Ther.*, 2018, **13**, 185–192.

42 D. Wo, J. Peng, D. N. Ren, L. Qiu, J. Chen, Y. Zhu, Y. Yan, H. Yan, J. Wu, E. Ma, T. P. Zhong, Y. Chen, Z. Liu, S. Liu, L. Ao, Z. Liu, C. Jiang, J. Peng, Y. Zou, Q. Qian and W. Zhu, Opposing Roles of Wnt Inhibitors IGFBP-4 and Dkk1 in Cardiac Ischemia by Differential Targeting of LRP5/6 and beta-catenin, *Circulation*, 2016, **134**, 1991–2007.

43 A. Vikram, Y. R. Kim, S. Kumar, A. Naqvi, T. A. Hoffman, A. Kumar, F. J. Miller Jr., C. S. Kim and K. Irani, Canonical Wnt signaling induces vascular endothelial dysfunction via p66Shc-regulated reactive oxygen species, *Arterioscler., Thromb., Vasc. Biol.*, 2014, **34**, 2301–2309.

44 J. Ma, Q. Cai, D. Yang, J. Yang, J. Xue, M. Yu, Y. Liu, F. Ma, F. Li and X. Liu, A Positive Feed Forward Loop between Wnt/beta-Catenin and NOX4 Promotes Silicon Dioxide-Induced Epithelial-Mesenchymal Transition of Lung Epithelial Cells, *Oxid. Med. Cell. Longevity*, 2020, **2020**, 3404168.

45 L. Zhou, X. Chen, M. Lu, Q. Wu, Q. Yuan, C. Hu, J. Miao, Y. Zhang, H. Li, F. F. Hou, J. Nie and Y. Liu, Wnt/beta-catenin links oxidative stress to podocyte injury and proteinuria, *Kidney Int.*, 2019, **95**, 830–845.

46 Y. Wang, L. Zheng, W. Shang, Z. Yang, T. Li, F. Liu, W. Shao, L. Lv, L. Chai, L. Qu, Q. Xu, J. Du, X. Liang, J. Zeng and J. Jia, Wnt/beta-catenin signaling confers ferroptosis resistance by targeting GPX4 in gastric cancer, *Cell Death Differ.*, 2022, **29**, 2190–2202.

47 J. Shen, Y. Li, Y. Jiao, J. Wang, X. Hou, Y. Su, B. Liu, H. Liu, Z. Sun, Q. Xi and Z. Fu, Wnt 3a Protects Myocardial Injury in Elderly Acute Myocardial Infarction by Inhibiting Serum Cystatin C/ROS-Induced Mitochondrial Damage, *Front. Physiol.*, 2022, **13**, 950960.

48 Z. Li, C. Chen, X. Zhu, Y. Li, R. Yu and W. Xu, Glycyrrhizin Suppresses RANKL-Induced Osteoclastogenesis and Oxidative Stress Through Inhibiting NF-kappaB and MAPK and Activating AMPK/Nrf2, *Calcif. Tissue Int.*, 2018, **103**, 324–337.

49 X. L. Li, A. G. Zhou, L. Zhang and W. J. Chen, Antioxidant status and immune activity of glycyrrhizin in allergic rhinitis mice, *Int. J. Mol. Sci.*, 2011, **12**, 905–916.

50 Y. Tang, X. L. Lv, Y. Z. Bao and J. R. Wang, Glycyrrhizin improves bone metabolism in ovariectomized mice via inactivating NF-kappaB signaling, *Climacteric*, 2021, **24**, 253–260.